Optimizing lunar regolith beneficiation for ilmenite enrichment

Kunal Kulkarni [1]*, Michel Fabien Franke [1],
Muchammad Izzuddin Jundullah Hanafi [2],
Thorsten M. Gesing [2,3] and Paul Zabel [1]

[1]German Aerospace Center, Institute of Space Systems, Bremen, Germany, [2]Institute of Inorganic Chemistry and Crystallography, University of Bremen, Bremen, Germany, [3]MAPEX Center for Materials and Processes, University of Bremen, Bremen, Germany

Over the past few years, the international space industry has focused extensively on advancing technologies to enable prolonged human space exploration missions. The primary limiting factor for these endeavors is the spacecraft's capacity to transport and store essential supplies from Earth to support human life and mission equipment throughout the mission's duration. *In-situ* resource utilization (ISRU) is the preferred solution for this challenge. Previous lunar missions have identified the presence of oxygen within the lunar regolith, which is an important resource for human space exploration missions. Oxygen is present in many different minerals within the lunar regolith out of which, ilmenite provides the highest yield of oxygen per unit mass using hydrogen reduction. However, the distribution of ilmenite is neither high nor uniform throughout the lunar surface and therefore, needs beneficiation, which is an important intermediate step for ilmenite-based oxygen production. A regolith beneficiation testbed was developed at DLR Bremen which is a TRL 4 level representation of the technology. The testbed has multiple process parameters that can be adjusted to produce the desired feedstock. This work focuses on the optimization of this testbed to produce a feedstock with higher ilmenite content than the input regolith. The testbed comprises three beneficiation techniques, viz. gravitational, magnetic and electrostatic beneficiation that work sequentially to produce the desired feedstock. The optimized parameter configuration achieved up to three-fold increase in the ilmenite grade relative to the input with about 32 wt% of the total ilmenite being recovered in the enriched output. These experiments have highlighted other underlying factors that influenced the experimental research such as the design of testbed components, system residuals and limited availability for Off-the-shelf components. The observations made from these experiments have also provided insights into the further development of the technology. The work has thus produced evidence for the effectiveness of the beneficiation testbed in producing an enriched feedstock while outlining avenues for future improvements.

KEYWORDS

ISRU, beneficiation, Moon, lunar regolith, simulants, ilmenite, oxygen extraction

1 Introduction

The choice of the Moon as the destination for upcoming space missions is primarily due to its greater accessibility compared to other celestial bodies, the *in situ* experience gained during the Apollo missions and the resources present in the lunar regolith that can be extracted and used for space exploration activities. The Apollo missions by NASA and the LUNA missions by ROSCOSMOS, being the initial participants for lunar exploration, were followed by international missions such as SMART-1 by ESA, SELENE by JAXA, CHANG'E by CNSA as well as the CHANDRAYAAN missions by ISRO (Sundararajan 2006; Colaprete et al., 2012); (Foing et al., 2005); (Ouyang et al., 2010). Upon analysis of all the mission data, it is clear that the lunar regolith contains essential minerals that can be utilized for future space missions. This led to the motivation of going back to the Moon with an intention of establishing a long-term human presence in space.

The utilization of space resources is the primary solution for enabling this vision and realizing this, the global space industry has taken major steps towards the development of ISRU technologies. The lunar regolith is the most abundant natural resource on the Moon which makes it a prime candidate of raw material for future ISRU missions. The minerals in lunar regolith contain high amounts of oxygen bonded in various forms such as silicates and oxides Click or tap here to enter text (Heiken et al., 1991). The capability of producing oxygen *in situ* is not only important for supporting human life but also to produce rocket fuel for further exploration. Out of all the available minerals, ilmenite (FeTiO3) provides the highest efficiency for extraction of oxygen per unit mass with hydrogen reduction (Gibson and Knudsen 1985). However, ilmenite is predominantly only found in the lunar mare regions with very scarce deposits in the lunar highlands making it difficult to make use of its higher yield (Heiken et al., 1991). Therefore, the excavated regolith will require additional processing for producing a feedstock with high ilmenite content that can be used for producing oxygen with improved process efficiency. This additional process is called beneficiation which involves the preparation of a consistent feedstock that is rich in the target mineral and is otherwise suited for the subsequent extraction process. The higher efficiency also translates to a lower energy demand for the same amount of oxygen produced.

Ilmenite-based production of oxygen is one of the most widely studied oxygen production techniques for ISRU technologies (Bunch et al., 1979; Gibson and Knudsen, 1985). Upon successful beneficiation, the ilmenite-rich feedstock will be further reduced by using molecular hydrogen producing iron, titanium oxide and water. Hydrogen and oxygen can then be produced by subsequent electrolysis of the produced water. The chemical reactions for both processes are shown in Eqs 1.1, 1.2 respectively.

$$FeTiO_3 + H_2 \rightarrow Fe + TiO_2 + H_2O \quad (1.1)$$

$$2H_2O \rightarrow 2H_2 + O_2 \quad (1.2)$$

Some early studies of lunar regolith beneficiation were done right after the Apollo and LUNA missions. In one such study a test bed was developed to examine the separation of metallic minerals using magnetic beneficiation (Agosto, 1981; Oder, 1991). The research provided a comprehensive feasibility analysis of the

magnetic beneficiation system for lunar regolith along with the necessary resources for its implementation in future space missions. The results from another study on regolith beneficiation for ilmenite enrichment show an average eleven-fold increase in the concentrations of ilmenite going from 7.9 wt% to 90 wt% after a single pass in a nitrogen environment with a reduced enrichment in vacuum conditions (Agosto, 1985). More recently, a concept called the Lunar Soil Particle Separator (LSPS) was proposed for beneficiation of lunar regolith (Berggren et al., 2011). It comprises different stages starting with a particle size separator followed by magnetic and electrostatic separation stages which is similar to the testbed used for experiments presented in this work. The experimental results from LSPS show an increase in the recovery and grade of target minerals such as iron oxides and ilmenite using the multi-stage sequential approach. In summary, prior research provides robust evidence for the efficacy of beneficiation techniques in concentrating specific lunar regolith materials, serving as benchmarks for this study, aiming to beneficiate the lunar regolith for producing a feedstock enriched with ilmenite.

2 Materials and methods

2.1 Experimental setup

The testbed used for the beneficiation experiments discussed within this research was developed at the DLR, Institute of Space Systems in Bremen (Franke, 2019). Figure 1 illustrates the fully assembled testbed highlighting the relevant components. The components are arranged vertically so that the gravitational force
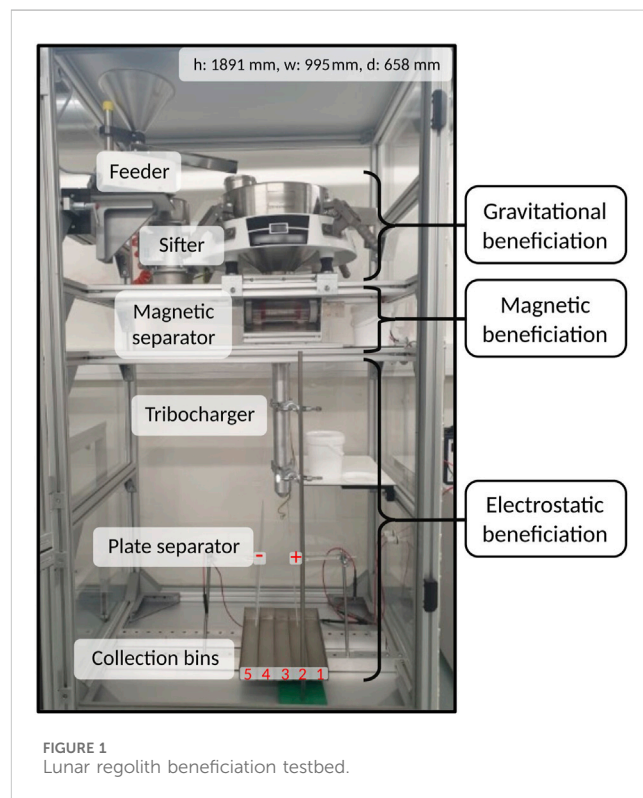

FIGURE 1
Lunar regolith beneficiation testbed.

is the primary mode of conveyance. The testbed has a height of 1891 mm, a width of 995 mm, and a depth of 658 mm. The entire setup is encapsulated in an assembly of aluminum profiles, plates, and various fixation elements.

Laborette 24, a vibratory feeder produced by *Fritsch GmBH* is the inlet for the testbed. This allows for a constant and controlled flow of regolith into the system. The feed rate can be adjusted manually using its control panel. The output of the feeder is a V-shaped channel that is connected to the further stages of beneficiation. The testbed comprises three beneficiation strategies: gravitational, magnetic, and electrostatic beneficiation respectively.

The first stage is gravitational beneficiation, which consists of the *Russel Compact Sieve*, a horizontal vibratory sifter used for the segregation of particles based on their size All particles with a diameter greater than 200 μm are removed at this stage. It is known from the Apollo samples that the ilmenite grain size ranges from 45–500 μm with highest concentrations in the 45–75 μm range (Heiken et al., 1991). Therefore the sifter indirectly increases the ilmenite grade while also achieving the correct feedstock size for subsequent processes.

The finer particles that are smaller than this threshold are transferred to the second stage of magnetic beneficiation. This stage uses a permanent magnet drum separator, developed at DLR Bremen, to segregate minerals based on their respective magnetic susceptibilities. It consists of an outer cylinder made from polycarbonate, which rotates at a user-defined rotational speed, and a stationary inner cylinder that holds permanent, arc-shaped neodymium-iron-boron (NdFeB) magnets. The fine particles from the sieve are fed into the magnetic separator from above, directly onto the rotating cylinder. As a result, the weakly magnetic particles fall off the drum sooner than the magnetic ones which remain adhered to the drum until they reach the last of the magnets and then get brushed off into a separate outlet. The goal of this stage is to remove the ferromagnetic agglutinates and metallic dust particles from the regolith leaving behind para- and diamagnetic minerals such as ilmenite, olivine, and other tailings.

These para- and dia-magnetic minerals are further transferred to the third stage of electrostatic beneficiation. The subprocess that is employed in the testbed's electrostatic separator is called tribocharging with plate separation. The tribocharger consists of a metallic spiral, which is used as an electrode to impart charge on the regolith particles via the triboelectric effect. This effect is directly related to the molecular content of the minerals. According to theory, the poorly chargeable ilmenite should retain little to no charge (due to its relatively high conductivity), while olivine and other tailings are expected to gain a net negative charge. A detailed analysis for the behavior of different regolith particles with tribocharging can be found in the testbed design document (Franke, 2019). The charged particles are then passed through a parallel plate separator that creates a homogeneous, high-voltage electrostatic field. Prior studies indicate a broad spectrum of field voltages that could be beneficial for ilmenite enrichment and are taken into consideration for the optimization experiments (Li et al., 1999; Trigwell et al., 2006; Trigwell et al. 2009; Trigwell et al. 2013). Due to the differences in developed charges, the particles are directed on different, distinguishable trajectories, which allows their collection in an array of bins with defined positions from

TABLE 1 List of adjustable process parameters of the beneficiation testbed.

Beneficiation stage	Process parameter	Unit	Range
Gravitational beneficiation	Feed rate	kg*h^{-1}	0–28.82
	Sieve size	μm	200[a]
Magnetic beneficiation	Motor rotational speed	rpm	0–1324
Electrostatic beneficiation	Electrostatic field voltage	kV	0–25
	Plate separation distance	mm	200[b]

[a]A different sieve size can be used but the current configuration remains fixed at 200 μm.
[b]The plate separation distance can be changed at regular intervals of 100 mm.

the center of the tribocharger outlet. For more details on the internal assembly design of the magnetic and electrostatic separators please refer the Supplementary Material document.

2.2 Beneficiation process parameters

The beneficiation testbed features a range of process parameters, as outlined in Table 1, which allow for adjustments to enhance the system's beneficiation performance. This study concentrates on optimizing three critical parameters: feed rate (f), motor rotational speed (ω_m), and electrostatic field voltage (V). To maintain consistency and minimize experimental variables during the initial optimization phase, the other parameters remain fixed.

2.3 Beneficiation performance quantification

The testbed's beneficiation performance is quantified through the utilization of parameters outlined in Table 2.

The yield and recovery together represent the material processing efficiency of the system while the grade and enrichment ratio indicate the degree of separation for ilmenite achieved with the beneficiation methods. An optimized system should exhibit good performance across both categories.

2.4 Lunar regolith simulants for experimental analysis

Analysis of samples from the Apollo missions indicates that the lunar mare regions generally contain a higher average ilmenite content in the regolith compared to the lunar highlands (Heiken et al., 1991). Hence, the LMS-1 simulant from *Exolith Lab* and the TUBS-M-based modular regolith from the *Technische Universität Berlin*, both representing the lunar mare regions, were consequently selected for the optimization experiments (Exolith Lab, 2014; Linke et al., 2020). The custom version of the TUBS-M-based modular regolith simulant used in this work is labeled as TMIA4 indicating the presence of TUBS-M base simulant, 4 wt% ilmenite, and agglutinates. Table 3 presents a comparative analysis of both simulants.

TABLE 2 Beneficiation parameters used for quantification of system performance Click or tap here to enter text (Hadler et al., 2020).

Parameter	Unit	Formula	Description
Yield	wt%	$\frac{M_{tm,o}}{M_i}$	The total mass of ilmenite in the output per unit mass of input material
Recovery	wt%	$\frac{M_{tm,o}}{M_{tm,i}}$	The mass of ilmenite in the output per unit mass of ilmenite in the input material
Grade	wt%	$\frac{M_{tm,o}}{M_o}$	The mass of ilmenite in the output per unit mass of output material
Enrichment ratio	-	$\frac{G_o}{G_i}$	Ratio of grade of ilmenite in the output material to the grade of ilmenite in the input material

TABLE 3 LMS-1 and TUBS-M based modular regolith simulant comparative analysis (Exolith Lab, 2014; Linke et al., 2020).

Parameter	LMS-1	TMIA4
Grain density [g/cm³]	2.92	2.96
Angle of repose [˚]	38.3	41.9–45.8
Ilmenite content [wt%]	4.03	4.00
Mean particle size [μm]	91	87
Particle size distribution [μm]	0.04–1000	0–2000

2.5 Characterization of experimental samples

2.5.1 X-ray powder diffraction analysis

Ilmenite rock, two lunar regolith simulants (LMS-1 and TUBS-M), and several samples from various input parameter configurations were ground for phase analysis by X-ray powder diffraction (XRPD). The data collection was carried out on a Bruker D8 DISCOVER X-ray diffractometer equipped with CuK$_{\alpha1,2}$ radiations ($\lambda_{K\alpha1}$ = 154.05929 (5) pm, $\lambda_{K\alpha2}$ = 154.4414 (2) pm) in Bragg–Brentano geometry. The data were collected at ambient conditions from 5˚ to 85˚ 2θ with a step width of 0.0149˚ 2θ and a measurement time of 0.42 s per step using an energy-discriminating LynxEye-XET multi-strip detector. Ilmenite rock sample was measured for longer time (7.7 s per step) to obtain better intensity to noise ratio. The Rietveld refinements of the XRPD data were performed using the available software suite (TOPAS V6.0, Bruker AXS). Rietveld refinement of ilmenite rock was used as a reference for phase quantification of the simulants and the experiment samples.

2.5.2 Microscopy

An additional elemental analysis was employed on the ilmenite sample by scanning electron microscopy/energy dispersive X-ray (SEM/EDX) spectroscopy. SEM was carried out using a JMS-6510 (JEOL) equipped with an X-Flash 410-M detector (Bruker) for EDX spectroscopy. A small amount of ilmenite was taken on conducting carbon tabs and sputtered with gold for 20 s with a JFC-1200 coater (JEOL) followed by inserting it into the SEM chamber.

2.6 Experimental approach

2.6.1 Systematic approach to planning and conducting experiments

A multi-phase optimization strategy is implemented to efficiently optimize the beneficiation testbed. Initially, all experiments are conducted with the LMS-1 simulant. In total, the experiments are categorized into four phases viz. phase 0, A, B, C, and D respectively. Phase 0 encompasses preliminary experiments and primarily validating the operational aspects of all testbed components. The insights gained from these experiments inform subsequent optimization efforts.

In phase A, the optimization of magnetic and gravitational beneficiation stages is achieved by conducting experiments across varying feed rates and rotational speeds of the magnetic separator while analyzing the beneficiation performance. This phase also aims to validate the magnetic separator's operational design.

Phases B and C concentrate on optimizing electrostatic beneficiation. Phase B investigates the output from the electrostatic plate separator across the entire range of possible field voltages. Phase C investigates the system output further across a field voltage range of ±2 kV relative to the optimum voltage from Phase B, determining the optimized process parameters for producing the desired feedstock.

Phase D is dedicated to validating system repeatability and reliability post-optimization. The optimized parameter configuration is applied to the TMIA4 simulant system, and the resulting beneficiation output is compared to phase C results. Any disparities in outcomes are examined to analyze the simulant-specific behavior of the beneficiation testbed, ultimately determining its applicability across diverse lunar regions.

Every experiment is conducted with a 300 g input sample. In order to compensate for experimental deviations, every configuration of process parameters is tested three times and the average of all the trials is considered for further analysis.

2.6.2 Experiment procedure

A standardized experimental procedure is adopted for the optimization to mitigate experimental variations thereby achieving reliable results. The procedure for this study is divided into multiple steps, each crucial for obtaining reliable and meaningful results.

The first step is sample preparation, which involves drying the simulant samples at 80˚C for a duration of 48 h. Once dried, they are stored in airtight containers to prevent moisture absorption. For each experiment, a consistent amount of 300 g of dried sample is then dispensed.

The second step, experiment machine setup, is essential to ensure accurate and controlled conditions. During this step, the machine parameters are configured according to the predefined process parameter settings for the specific experiment. Subsequently, the dried sample is loaded into the feeder, which marks the readiness for the experimental run.

FIGURE 2
Experimental procedure for optimization of beneficiation testbed.
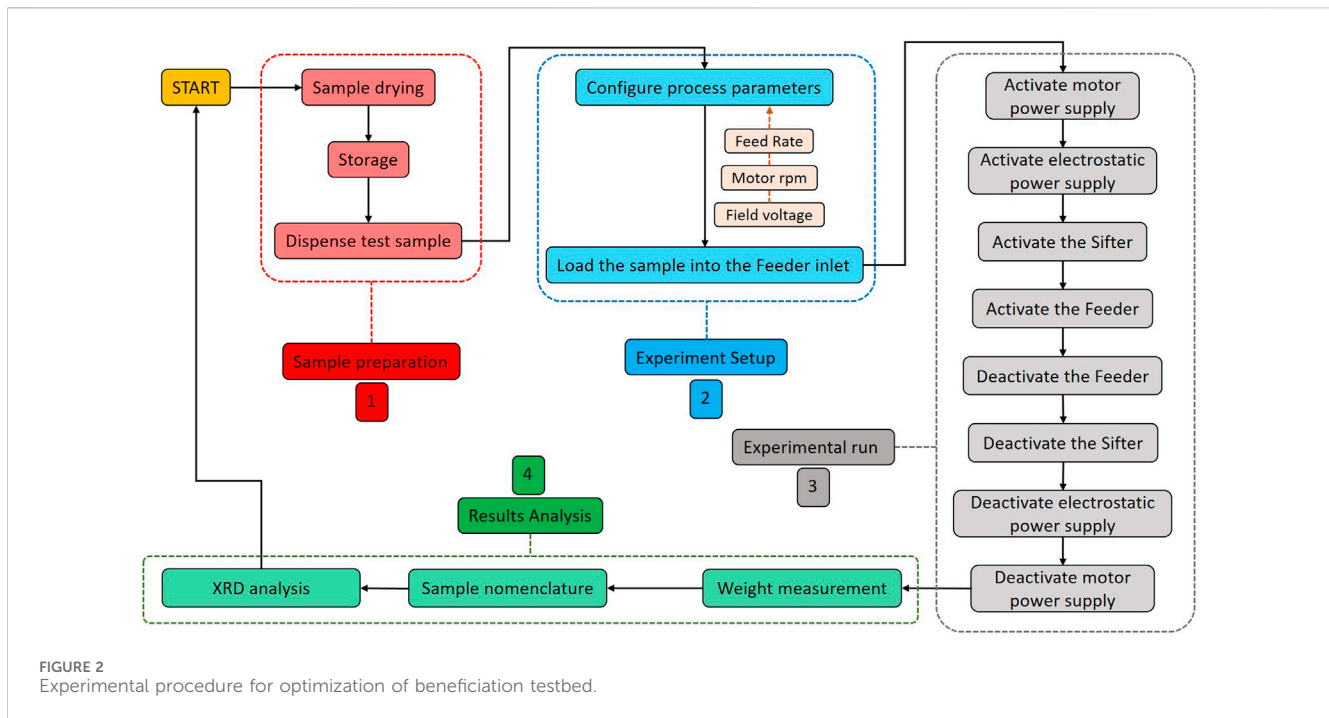
The third step, the experimental run, is the core of the procedure. This is where the actual experiment is conducted based on the set parameters. It involves activating different stages of beneficiation in a predefined sequence to process the sample thoroughly.

The final step, results analysis, is critical for interpreting and understanding the outcomes. Firstly, all system outlets are carefully weighed. The collected samples undergo XRPD analysis, which provides insights into the mineral composition and phase characteristics of the samples. The diffraction intensities are directly related to crystal structure and the amounts of each phase, hence a precise quantitative analysis with detection limit of 1.3 wt% is yielded from the well-known Rietveld method (Bish and Chipera, 1994; Reid and Hendry, 2006; Bish and Plötze, 2010; Xie et al., 2017). The XRPD results are used for analyzing system beneficiation performance using the performance parameters discussed in Section 3.3. Figure 2 gives an overview of the experimental procedure.

3 Results

3.1 Ilmenite characterization

In order to identify the elements, present in an ilmenite sample, a SEM/EDX analysis was conducted. Selected electron micrographs of ilmenite powder are provided in Figure 3. EDX spectra were analyzed for concentration of different elements contained in ilmenite. It can be inferred that there is a dominance of titanium and iron (69 and 28 wt%, respectively) in the tested samples.

X-ray powder data Rietveld refinement were employed to have a precise phase quantification of the sample. This characterization method confirms that ilmenite rock comprises of 12 phases. Among them, rutile (TiO_2), moganite (SiO_2), iron titanium oxide (($FeTiO_3$)$_{0.8}$(Fe_2O_3)$_{0.2}$) and hematite (Fe_2O_3) can be considered as major phase (>10 wt%). These

FIGURE 3
Representative scanning electron micrographs of ilmenite sample.
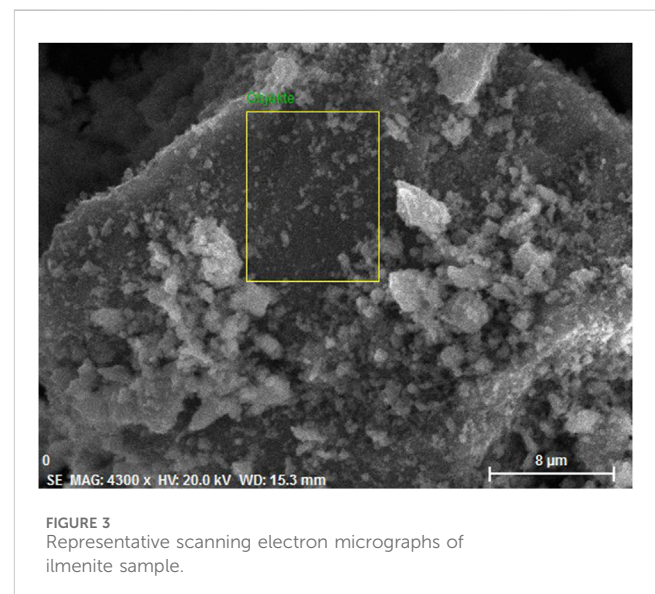
four major ilmenite-associated phases were summed as reference and designated as grade (see Section 2.3) to quantify the Lunar simulants and output testbed samples. XRPD Rietveld refinement plot of the tested ilmenite sample is given in Figure 4.

3.2 Lunar simulants characterization

Lunar simulants of TMIA4 and LMS-1 were subjected to XRPD characterization to examine the presence of four major ilmenite-associated phases. XRPD Rietveld plots of both simulants are depicted in Figures 5, 6. Several phases such as enstatite ferroan,
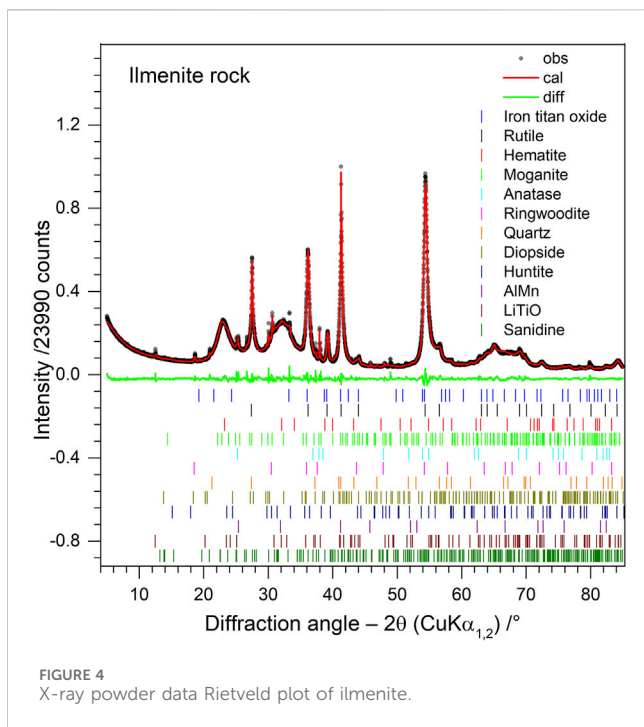
FIGURE 4
X-ray powder data Rietveld plot of ilmenite.

FIGURE 6
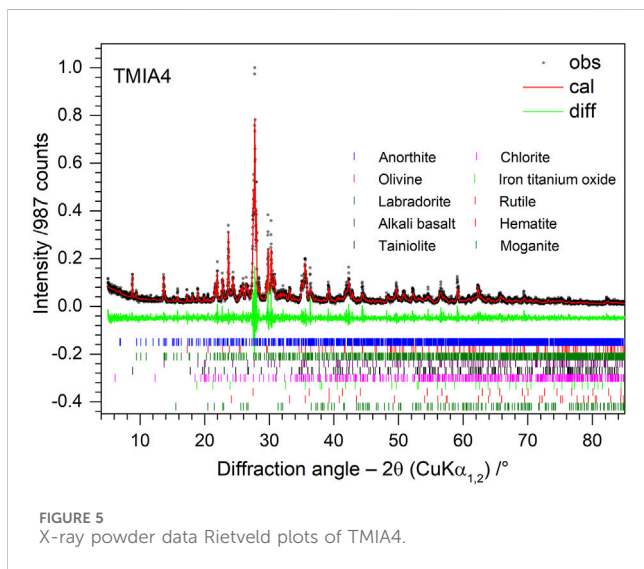X-ray powder data Rietveld plots of LMS-1.

FIGURE 5
X-ray powder data Rietveld plots of TMIA4.

quartz, chabazite, and amphibole were only found in LMS-1. Among the main interests, all four major ilmenite-associated phases were identified in TMIA4, whereas LMS-1 does not contain any hematite. The phase quantifications give approximately 2.8 (4) and 1.6 (2) wt% grade of ilmenite in TMIA4 and LMS-1, respectively. The numbers in brackets are the calculated estimated standard deviations of the obtained values in the last digit.

3.3 Phase 0: preliminary experiments

The primary aim of the preliminary experiments was to test the operational designs of the testbed components and ensure their
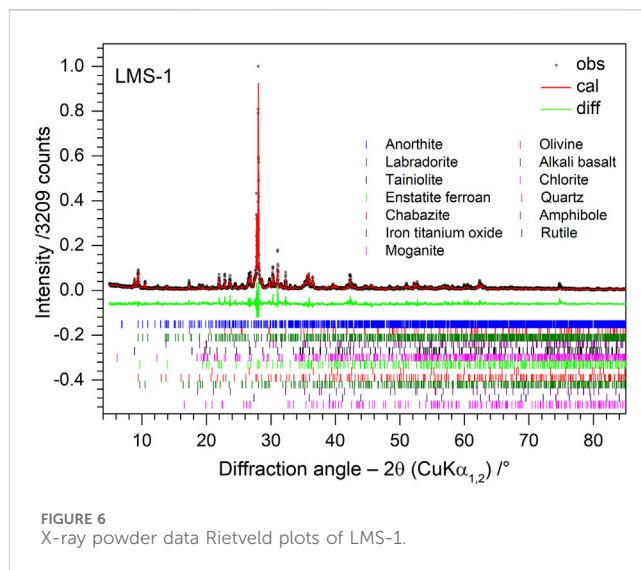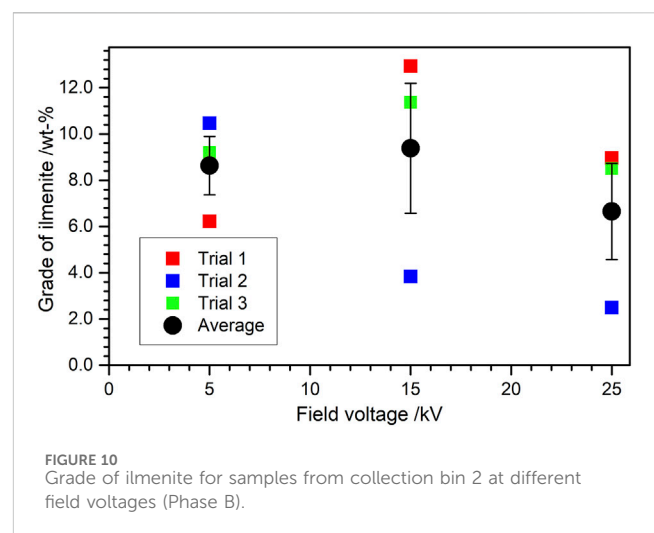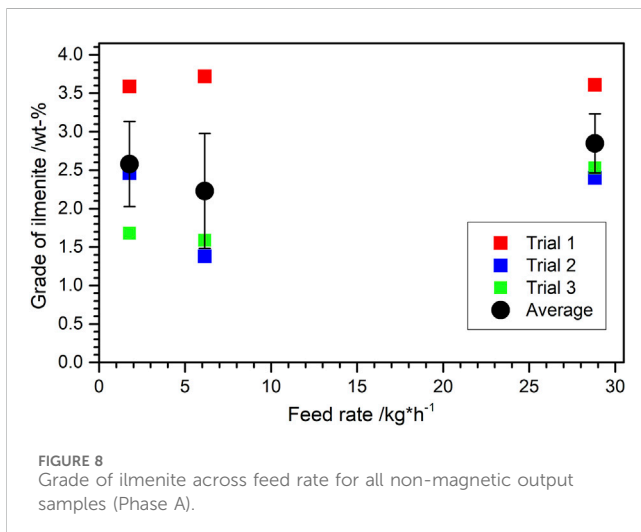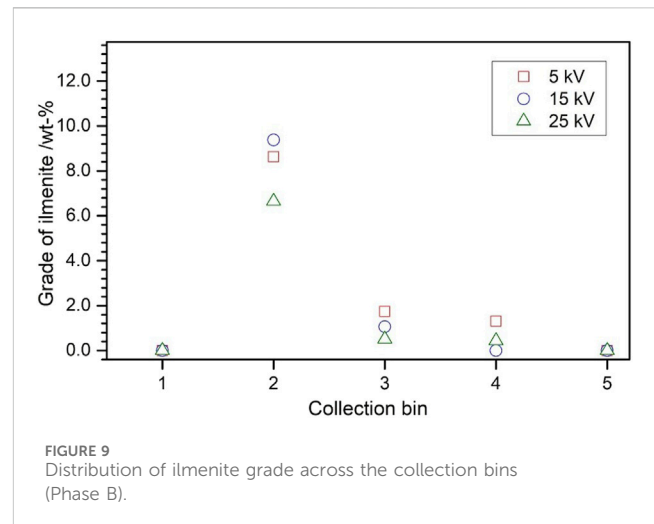
functionality. It was observed that at feed rates lower than $6.14 \, \text{kg*h}^{-1}$, the dust build-up on the feeder output rail is significant and reduces the effective feed rate. This corresponds to a higher maintenance frequency for cleaning the output rail and retaining the processing speed. Moreover, a major challenge was observed with magnetic beneficiation. The selected motor configuration did not possess the requisite torque, limiting the adjustment of rotational speeds. Consequently, the optimization experiments were confined to a fixed rotational speed of 794 rpm for the magnetic separator.

3.4 Phase A: optimization of gravitational and magnetic beneficiation

The primary aim of this phase is to study the effects of changing feed rate and rotational speeds on the beneficiation outcome. As the preliminary experiments concluded, the magnetic separator's rotational speed remains fixed at 794 rpm due to design limitations. Therefore, experiments are performed at different feed rates. The samples from the magnetic and non-magnetic outputs are analyzed for beneficiation performance. Figure 7 shows the average grade of ilmenite at different feed rates for the magnetic and non-magnetic output samples. It can be seen that the average grade of ilmenite for the non-magnetic output is in the range of 2.23–2.85 wt% while that in the magnetic output is in the range of 0.37–0.77 wt%. This validates the ability of the magnetic beneficiation stage to remove ferromagnetic agglutinates from the regolith leaving behind most of the ilmenite in the non-magnetic output.

Figure 8 illustrates the ilmenite grade within the non-magnetic output samples at different feed rates. Across the entire range of tested feed rates, the average grade of ilmenite varies only by 0.62 wt% with a minimum of 2.23 wt% and a maximum of 2.85 wt%. This indicates that variation in feed rate has less impact on the average ilmenite grade. Consequently, these findings lead to the conclusion that, within the testbed, the feed rate exerts minimal influence on the magnetic separator's

FIGURE 7
Average grade of ilmenite at varying feed rates (Phase A).

FIGURE 9
Distribution of ilmenite grade across the collection bins
(Phase B).

FIGURE 8
Grade of ilmenite across feed rate for all non-magnetic output
samples (Phase A).

FIGURE 10
Grade of ilmenite for samples from collection bin 2 at different
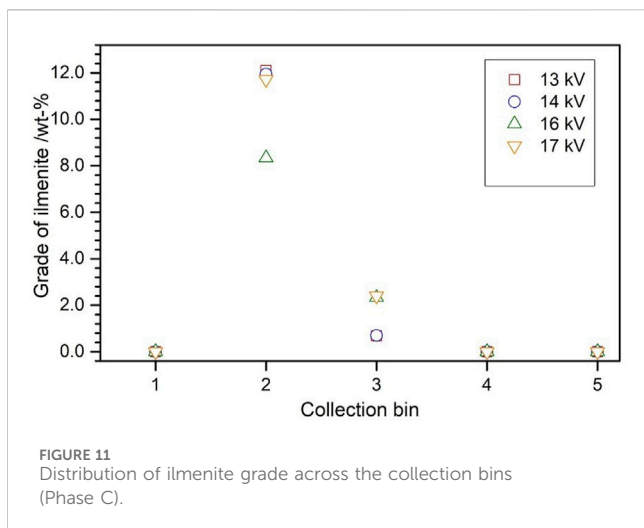field voltages (Phase B).
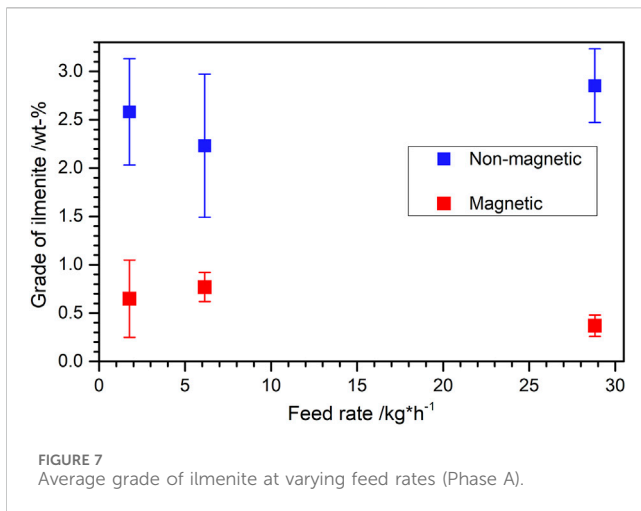
beneficiation performance. Considering the increased maintenance frequency observed at lower feed rates during the preliminary experiments as well as the material processing capacity for the magnetic separator which cannot process high amount of regolith at the same time due to its smaller dimensions, the value of 6.14 kg*h^{-1} is chosen with the rotational speed of 794 rpm for further optimization.

3.5 Phase B: optimization of electrostatic beneficiation (first iteration)

This phase of optimization focuses on the electrostatic beneficiation stage, specifically the voltage of the electrostatic parallel plate separator. It was decided to test the beneficiation performance across all available field voltages from 0–25 kV and analyze the results. This is split into two stages. The first iteration (Phase B) involves experiments at larger intervals to encompass the entire available range. The next iteration (Phase C) will then choose a narrower range depending on the results from this phase of experiments.

An important aspect of understanding the effectiveness of electrostatic beneficiation is to determine the distribution of ilmenite across the five collection bins. This examination aims to identify the bin with the highest ilmenite concentration, thereby yielding the desired enriched feedstock. As shown in Figure 9, it is observed that the grade of ilmenite in bin 2 lies in the range of 6.65–9.38 wt% across all tested field voltages. In contrast to this, the grade of ilmenite in bins 3 and 4 lies in the range 0.44–1.74 wt% which is much lower compared to the samples from bin 2. Moreover, the bins 1 and 5 collect no sample material in any of the experimental configurations. Therefore, collection bin 2 is considered as the desired output with ilmenite-enriched feedstock. As a result, further analyses are performed with samples from the collection bin 2.

Figure 10 shows the grade of ilmenite for samples from collection bin 2 at varying field voltages. The plotted average data points exhibit a consistent rise in grade from 8.63 wt% to 9.38 wt% when increasing the field voltage from 5 to 15 kV, followed by a decrease to 6.65 wt% at 25 kV. Based on this analysis, it is concluded that field voltages near 15 kV are more likely to produce the desired

FIGURE 11
Distribution of ilmenite grade across the collection bins (Phase C).

FIGURE 12
Grade of ilmenite for samples from collection bin 2 at different field voltages (Phase C).

results. Consequently, 15 kV is chosen as the reference for the next iteration of optimization.

3.6 Phase C: optimization of electrostatic beneficiation (second iteration)

The phase C experiments follow a similar procedure as in phase B, focusing on a narrower range of field voltages. Given the favorable beneficiation outcomes achieved at 15 kV, it serves as the reference point. Consequently, a range spanning from 13 kV to 17 kV is chosen, with a testing interval of 1 kV. The objective is to assess the testbed's beneficiation performance within this smaller voltage range and determine the optimized field voltage value.

An analysis of the ilmenite grade across all collection bins is conducted to reaffirm the earlier findings. As depicted in Figure 11, the results align closely with the previous analysis with an ilmenite grade between 11.71–12.10 wt% in bin 2 while only about 0.68–2.33 wt% in bin 3 with no material collected in bins 1, 4 and 5. As the collection bin 2 consistently exhibits a higher average ilmenite grade, only the samples from bin 2 are considered for subsequent analyses.

Figure 12 illustrates the grade of ilmenite across the narrower range of field voltages (13–17 kV). The grade of ilmenite does not follow a consistent trend in this narrow range and therefore, it is not independently conclusive about the most optimum configuration of process parameters for producing the desired feedstock.

Therefore, a trade-off between the four beneficiation parameters is conducted for all samples collected in bin 2 at the field voltages used in this phase. The results of experiments performed at 15 kV from the previous phase are also considered for reference. Table 4 shows the beneficiation parameters at different field voltages. It is observed that at 13 kV, the system produces the highest concentration of ilmenite indicated by the grade of 12.10 wt% and enrichment ratio of 3.00. This shows a higher degree of separation for ilmenite achieved at 13 kV. In contrast to this, at 17 kV, the yield and recovery are the highest at 1.33 wt% and 33.00 wt%, respectively, indicating a higher material processing efficiency. However, this also translates to the recovery of more
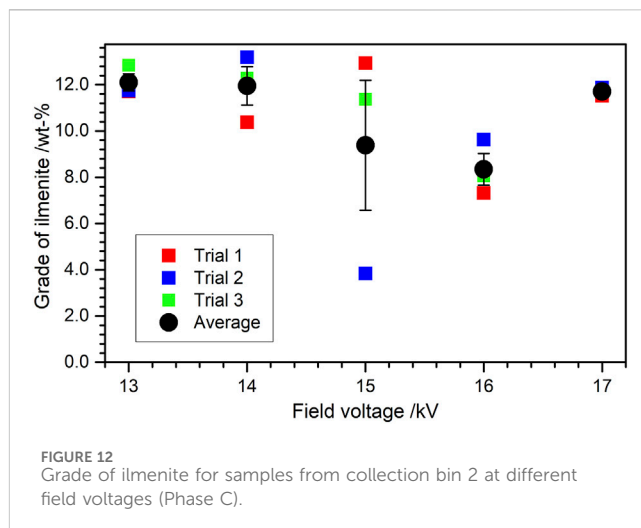
unwanted material which is indicated by the reduced grade and enrichment ratio of 11.71 wt% and 2.90, respectively.

An optimized solution, considering all the relevant factors, is evident at 14 kV. This configuration yields an ilmenite yield of 1.29 wt%, a recovery of 31.93 wt%, a grade of 11.95 wt%, and an enrichment ratio of 2.96, representing the second-highest values across all the beneficiation performance parameters. Therefore, the final optimized configuration of parameters derived from the experiments in phases A, B, and C is established as follows: f = 6.14 kg*h^{-1}, ω_m = 794 rpm, and V = 14 kV.

3.7 Phase D: validation of optimized configuration with TMIA4 simulant

The phase D experiments are focused on the validation of the optimized performance of the beneficiation testbed on a different simulant. The aim is to test the repeatability and reliability of results generated in the previous experiments. The experiments in this phase are performed with the TMIA4 simulant using the optimized parameter configuration from the phase C results.

The first step of this validation is to study the distribution of ilmenite across the collection bins and compare it to the previous results. As shown in Figure 13, similarly to previous results the collection bin 2 has a higher average ilmenite grade varying between 7.97–9.07 wt% across all the trials. However, the grade of ilmenite in bin 3 is higher than that in the previous experiments. The average grade of ilmenite in bin 3 is 5.64 wt% at 14 kV which is eight times more than that as seen with LMS-1. This indicates a potential for further optimization of the process with TMIA4.

A comparative analysis of the beneficiation parameters for ilmenite with the optimized parameter configuration from phase D with TMIA4 simulant and phase C with LMS-1 simulant is illustrated in Table 5. The LMS-1 simulant demonstrates a higher degree of separation of ilmenite evidenced by the grade of 11.95 wt% and enrichment ratio of 2.96 which are both higher than that of TMIA4. However, TMIA4 exhibits a higher efficiency of material processing which is evidenced by the higher yield of 1.49 wt% and recovery of 37.02 wt% in the produced feedstock. One of the factors

TABLE 4 Beneficiation parameters for ilmenite at different field voltages with standard error in brackets (Phase C).

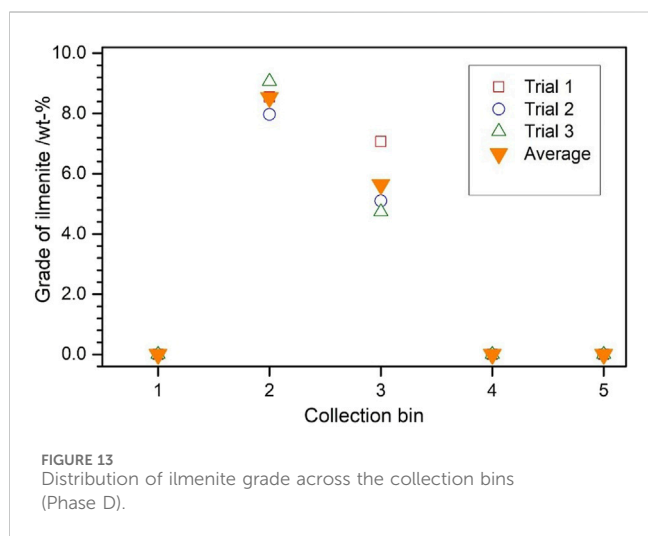| Field Voltage/kV	Yield/wt%	Recovery/wt%	Grade/wt%	Enrichment ratio
13	0.84 (0.12)	20.78 (2.96)	12.10 (0.37)	3.00 (0.09)
14	1.29 (0.27)	31.93 (6.69)	11.95 (0.82)	2.96 (0.20)
15	1.28 (0.79)	31.76 (19.59)	9.38 (2.8)	2.33 (0.69)
16	1.10 (0.26)	27.22 (6.46)	8.34 (0.68)	2.07 (0.16)
17	1.33 (0.55)	33.00 (13.55)	11.71 (0.10)	2.90 (0.02)

FIGURE 13
Distribution of ilmenite grade across the collection bins
(Phase D).

TABLE 5 Comparison of beneficiation results with LMS-1 and TMIA4 with standard error in brackets.

Beneficiation parameter	LMS-1	TMIA4
Yield/wt%	1.29 (0.27)	1.49 (0.58)
Recovery/wt%	31.93 (6.69)	37.02 (14.46)
Grade/wt%	11.95 (0.82)	8.53 (0.31)
Enrichment Ratio	2.96 (0.20)	2.11 (0.07)

for this discrepancy is the higher aspect ratio of particles in the TMIA4 simulant compared to that of the LMS-1 (Exolith Lab, 2014; Linke et al., 2020). However, further experiments with TMIA4 are indeed necessary for making more reliable claims about the simulant-dependent behavior of the beneficiation testbed. These results reveal a comparable beneficiation performance of the system across both the simulant systems.

4 Discussion

The experiments encountered specific limitations that prevented the complete optimization of the system. One major challenge was experienced with the selected motor configuration for the magnetic separator. The selection primarily revolved around the necessary rotational speed, but the final assembly revealed a lack of torque provided by the motor. Consequently, the rotational speed of the magnetic separator remained fixed, and optimization of this stage could not be undertaken within the scope of this study. Another limitation of this research was regarding the smaller sample size of three trials for every parameter configuration. This is reflected in the deviations seen from the experimental results. The experimental deviations can also be attributed to the in-homogeneity of the regolith simulants which could not be verified within the scope of this research. These limitations should be taken into consideration while evaluating future beneficiation experiments.

A peculiar observation was made during the optimization experiments regarding the system residuals. Despite ensuring a clean setup for each new parameter configuration to prevent sample contamination, it was consistently observed that the amount of residuals decreased and eventually stabilized at a constant level with each experimental run. This phenomenon suggests that the system residuals can reach a saturation point over time, maintaining a steady state during continuous operation. Consequently, this observation hints at the possibility of improving the system's material processing efficiency, potentially resulting in more consistent system performance.

This work also underscores the influence of constraints associated with the availability of off-the-shelf equipment for the particle sizing stage of the testbed, which initially led to high residuals. During the testbed development phase, the majority of available commercial vibratory sifters had high processing capacities, and therefore the choice was made with the lowest possible alternative. However, this led to substantial residuals when used with smaller batches as discussed in this work, which negatively impacted material processing efficiency, a concern that would otherwise be neglected with larger batches. Therefore, future developments in ISRU technologies, particularly those dealing with processing planetary regoliths, will need additional alternatives to address the disparity between equipment demand and supply.

In regards to the future implementation of a beneficiation system on the lunar surface, multiple variables need to be considered. First of all, the reduced gravity on the lunar surface will affect such a system to high degrees. Specifically, the processing speed of the setup will likely decrease due to reduced gravitational acceleration. However, the reduced speed will benefit the electrostatic beneficiation stage as the particles will travel longer through the electrostatic fields, providing more time for the field forces to deflect their trajectories further apart from each other. Moreover, the vacuum environment is claimed to improve the

beneficiation performance further according to previous research (Agosto, 1985). However, in orderto support the oxygen production infrastructure of an entire lunar base, the feedstock requirements are expected to be in the order of tons every day (Cilliers et al., 2020; Colozza, 2020; Cilliers et al., 2020). The current design has limitations to its scalability to support such infrastructures and would need to be considered for future developments of the system. Upon successful scaling up of the design, the expected outcomes are expected to show similar or even better results as the relative quantity of residual material reduce with increased overall processing quantity.

It should be noted that while this research focuses on ilmenite as the target mineral, the underlying principles of beneficiation can be extended to the processing of other minerals present in lunar or even martian regoliths too whichopens up more avenues for future research and development in the field.

5 Conclusion and outlook

The experimental analysis of the lunar regolith beneficiation testbed has yielded promising results and the optimization process was successful in identifying the optimal configuration of process parameters for producing an ilmenite-rich feedstock. It is evident from this analysis that the improvement in beneficiation parameters of the produced feedstock takes place gradually with every optimization phase. The grade of ilmenite in the output went from 2.55 wt% in phase A to 9.00 wt% in phase B and further to 12.00 wt% in phase C. A similar increase of enrichment ratio from 0.71 in phase A, to 2.33 in phase B and 2.96 in phase C is observed. This demonstrates the effectiveness of the developed strategy in optimizing the beneficiation performance of the testbed. The final results show that up to 32 wt% of the total ilmenite from the input regolith simulant is recovered in the produced feedstock with the optimized parameter configuration.

The total time for processing 300 g of regolith simulant is about 30 min resulting in an average energy consumption of about 61 Wh for the entire testbed. The discovery of the peculiar crystal structure of ilmenite used in the regolith simulants was also accomplished during the XRPD measurements. This analysis will further enable the development of processing techniques for lunar as well as other planetary regoliths.

In summary, this work has successfully demonstrated the feasibility as well as optimization capabilities of a small-scale, TRL 4 lunar regolith beneficiation testbed. Through a systematic approach, the process parameters of the system have been investigated and refined to achieve improved beneficiation outcomes. The optimization experiments have demonstrated the effectiveness of the testbed in producing ilmenite-rich feedstock, with measurable improvements observed in the grade, recovery, and enrichment ratio of ilmenite. The comparative analysis of different simulant systems highlights the adaptability and repeatability of the implemented beneficiation processes. In summary, the authors anticipate that this study will enhance comprehension of the optimization of lunar regolith beneficiation processes and offer insights into prospective research directions and practical applications in the realm of space exploration and resource utilization.

Data availability statement

The raw data supporting the conclusions of this article will be made available by the authors, without undue reservation.

Author contributions

KK: Formal Analysis, Investigation, Methodology, Writing–original draft, Writing–review and editing. MF: Writing–original draft. MJ: Writing–original draft. TG: Writing–review and editing. PZ: Writing–review and editing.

Funding

Acknowledgments

Conflict of interest

The authors declare that the research was conducted in the absence of any commercial or financial relationships that could be construed as a potential conflict of interest.

Publisher's note

All claims expressed in this article are solely those of the authors and do not necessarily represent those of their affiliated organizations, or those of the publisher, the editors and the reviewers. Any product that may be evaluated in this article, or claim that may be made by its manufacturer, is not guaranteed or endorsed by the publisher.

Supplementary material

The Supplementary Material for this article can be found online at: https://www.frontiersin.org/articles/10.3389/frspt.2023.1328341/full#supplementary-material

References

Agosto, W. N. (1981). "Beneficiation and powder metallurgical processing of lunar soil metal," in 4th Space manufacturing; Proceedings of the Fifth Conference, Princeton, NJ, USA, May, 1981.

Agosto, W. N. (1985). Electrostatic concentration of lunar minerals. Available online at https://ui.adsabs.harvard.edu/abs/1985lbsa.conf.453A/abstract.

American Institute of Aeronautics and Astronautics (1981). "Space manufacturing 4," in 4th Space manufacturing; Proceedings of the Fifth Conference, Princeton, NJ, USA, May, 1981.

American Institute of Aeronautics and Astronautics (2011). "Aerospace Sciences meetings," in 49th AIAA Aerospace Sciences Meeting including the New Horizons Forum and Aerospace Exposition, Orlando, Florida, USA, January, 2011.

Berggren, M., Zubrin, R., Jonscher, P., and Kilgore, J. (2011). "Lunar soil particle separator," in 49th AIAA Aerospace Sciences Meeting including the New Horizons Forum and Aerospace Exposition, Orlando, Florida, USA, January, 2011.

Bish, D. L., and Chipera, S. J. (1994). Accuracy in quantitative X-ray powder diffraction analyses. Adv. x-ray Anal. 38, 47–57. doi:10.1154/S0376030800017638

Bish, D. L., and Plötze, M. (2010). "X-Ray powder diffraction with emphasis on qualitative and quantitative analysis in industrial mineralogy," in Giovanni ferraris. Editor G. E. Christidis (European Mineralogical Union and the Mineralogical Society of Great Britain & Ireland), 35–76. doi:10.1180/EMU-notes.9.3

Bunch, T. E., Williams, R. J. P., Mckay, D. S., and Giles, D. (1979). Mining and beneficiation of lunar ores. Available online at https://ui.adsabs.harvard.edu/abs/1979srss.rept.275B/abstract.

Captain, J. G., Arens, E. E., Quinn, J. W., and Calle, C. I. (2009). The use of tribocharging in the electrostatic beneficiation of lunar simulant. IEEE Trans. Ind. Appl. 45 (3), 1060–1067. doi:10.1109/TIA.2009.2018976

Cilliers, J. J., Rasera, J. N., and Hadler, K. (2020). Estimating the scale of Space Resource Utilisation (SRU) operations to satisfy lunar oxygen demand. Planet. Space Sci. 180, 104749. doi:10.1016/j.pss.2019.104749

Colaprete, A., Elphic, R. C., Heldmann, J., and Ennico, K. (2012). An overview of the lunar crater observation and sensing satellite (LCROSS). Space Sci. Rev. 167 (1-4), 3–22. doi:10.1007/s11214-012-9880-6

Colozza, J. A. (2020). Small lunar base camp and in situ resource utilization oxygen production facility power system Comparison. Available online at https://ntrs.nasa.gov/citations/20200001622.

Exolith Lab (2014). "LMS-1 lunar mare simulant: fact sheet," in Dictionary geotechnical engineering/wörterbuch GeoTechnik. Editors Herrmann H. and Herbert B. (Berlin, Heidelberg: Springer Berlin Heidelberg), 603.

Franke, M. (2019). Development of a testbed for the beneficiation of lunar regolith. Available online at https://elib.dlr.de/185548/1/MA_SpaceEngineering_Franke_3218889_Digital2.pdf.

Gibson, M. A., and Knudsen, C. W. (1985). Lunar oxygen production from ilmenite. Available online at https://adsabs.harvard.edu/full/1985lbsa.conf.543G.

Hadler, K., Martin, D. J. P., Carpenter, J., Cilliers, J. J., Morse, A., Starr, S., et al. (2020). A universal framework for space resource utilisation (SRU). Planet. Space Sci. 182, 104811. doi:10.1016/j.pss.2019.104811

Heiken, G. H., Vaniman, D. T., and French, B. M. (1991). Lunar sourcebook: a user's guide to the Moon. Available online at https://www.lpi.usra.edu/publications/books/lunar_sourcebook/pdf/LunarSourceBook.pdf.

Herrmann, H., and Bucksch, H. (2014). Dictionary geotechnical engineering/wörterbuch GeoTechnik. Berlin, Germany: Springer Berlin Heidelberg.

Li, T. X., Ban, H., Hower, J. C., Stencel, J. M., and Saito, K. (1999). Dry triboelectrostatic separation of mineral particles: a potential application in space exploration. J. Electrost. 47 (3), 133–142. doi:10.1016/S0304-3886(99)00033-9

Linke, S., Windisch, L., Kueter, N., Wanvik, J. E., Voss, A., Stoll, E., et al. (2020). TUBS-M and TUBS-T based modular Regolith Simulant System for the support of lunar ISRU activities. Planet. Space Sci. 180, 104747. doi:10.1016/j.pss.2019.104747

Oder, R. R. (1991). Magnetic separation of lunar soils. IEEE Trans. Magn. 27 (6), 5367–5370. doi:10.1109/20.278841

Reid, J. W., and Hendry, J. A. (2006). Rapid, accurate phase quantification of multiphase calcium phosphate materials using Rietveld refinement. J. Appl. Crystallogr. 39 (4), 536–543. doi:10.1107/S0021889806020395

Space, (2006). Space. Reston, Virgina: American Institute of Aeronautics and Astronautics.

Sundararajan, V. (2006). "International missions to the Moon: space exploration goals, programs and economics," in Space 2006, Reston, Virigina: American Institute of Aeronautics and Astronautics.

Trigwell, S., Captain, J., Captain, J., Ellen, A., Quinn, J., and Calle, C. I. (2006). Electrostatic beneficiation of lunar simulant. Available online at https://ntrs.nasa.gov/citations/20130011155.

Trigwell, S., Captain, J., Weis, K., and Quinn, J. (2013): Electrostatic beneficiation of lunar regolith: applications in in situ resource utilization. In J. Aerosp. Eng. 26 (1), pp. 30–36. doi:10.1061/(ASCE)AS.1943-5525.0000226

Xie, R., Li, Y., Liu, H., and Zhang, X. (2017). Insights into the structural, microstructural and physical properties of multiphase powder mixtures. J. Alloys Compd. 691, 378–387. doi:10.1016/j.jallcom.2016.08.266

Nomenclature

DLR	Deutsches Zentrum für Luft- und Raumfahrt
ISRU	In-Situ Resource Utilization
ESA	European Space Agency
JAXA	Japanese Aerospace Exploration Agency
NASA	National Aeronautics and Space Administration
ISRO	Indian Space Research Organisation
CNSA	China National Space Administration
XRPD	X-Ray Powder Diffraction
SEM/ EDX	Scanning electron microscopy with Energy dispersive X-ray spectroscopy
M_i	Total mass of unprocessed raw material at the input
M_o	Total mass of processed material at the output
$M_{tm,i}$	Mass of target mineral in input
$M_{tm,o}$	Mass of target mineral in output
G_i	Grade of target mineral in input
G_o	Grade of target mineral in output